BOEING AEROSPACE COMPANY
A Division of The Boeing Company

P.O. Box 3999
Seattle, Washington 98124-2499

(2)

SINGLE EVENT UPSET TESTING

FINAL REPORT;

Tommy L. Criswell
Dennis L. Oberg
Jerry L. Wert
Paul R. Measel

March 1988

Naval Research Laboratory

N00014-85-C-2622

Prepared by

The Boeing Company

P.O. Box 3999

Seattle, WA 98124

BOEING

SINGLE EVENT UPSET TESTING

Tommy L. Criswell, Dennis L. Oberg

Jerry L. Wert, and Paul R. Measel

Abstract

This Final Report presents the results of an experimental program to characterize single event upset phenomena in selected bipolar memory devices irradiated with relativistic heavy ions. The principal objective was to determine the multibit upset rate at normal and parallel beam incidence angles. The impetus for this objective is that multibit errors are not generally detectable by the simple Hamming codes currently used on spacecraft. Multibit errors significantly reduce spacecraft reliability by initiating spurious commands. It was found in this program that the multibit error cross section is equal to or greater than the projected area of the depletion regions for parallel and for normal to 60 degree incidence beams.

In conducting these tests it was found that for some devices the cross section and critical LET do not scale as the secant of the incidence angle or with the dose-averaged LET. Current SEU testing and analysis techniques have as basic assumptions that the charge deposited at a junction depends linearly on the stopping power of the ion and the pathlength of the ion through an imagined parallelepiped that represents the depletion region. This study tested these assumptions for two bipolar parts, AMD 27LS00 and Fairchild 93L422, by irradiating at fixed angles while varying the LET of two ion species. It was found that the 27LS00 shows a pronounced ion species dependence, and may show a deviation of deposited charge from the usual

secant times a fixed depletion depth, while the 93L422 exhibited the expected secant dependence and no ion species dependence.

In addition, as called for in the statement of work, dosimetry support was given in the irradiation of an RCA arithmetic logic unit with a beam that simulated the iron component of the galactic cosmic ray iron spectrum.

Introduction

Multibit errors resulting from a single ion hitting a device potentially provide a severe failure mode because they defeat the use of Hamming code to protect data. Multibit errors have been observed on TDRS,[1] on low-altitude polar orbit satellites,[2] and Pioneer Venus 1.[3] On these platforms the multibit SEU's are on the order of 2% of the total number of SEU's. Some planned spacecraft[4] have memory arranged with all bits of a word on the same chip. Such arrangements are particularly susceptible to multibit SEU.

A previous paper[5] discussed the development of a new experimental method for SEU testing using relativistic heavy ions from the Lawrence Berkeley Laboratory Bevalac. This report presents results of the continuing experiments to utilize the unique properties of this accelerator facility for SEU testing. Relativistic heavy ions used in this work are highly penetrating with ranges in silicon spanning from millimeters to a few centimeters. For the devices tested the LET of the beam does not change in penetrating overlayers or traversing the sensitive volume, even at high incidence angles. The devices themselves have sensitive junctions (the collector/substrate junction in this case) with areal dimensions large compared to their thicknesses. As seen in figure 1, the range in LET covered by a single ion species is large and covers the range of ion energies typical of galactic cosmic rays. SEU cross

sections may then be measured at fixed incidence angles while varying LET by varying the ion energy. Variations from the secant dependence of the projected sensitive junction area and deposited charge can be detected. Whether the causes of the variations are due to angle dependent charge collection from the funnel or from an ion shunt can not be determined without measuring the time dependence of the SEU current at all memory cell nodes. Such pulse shape measurements were beyond the scope of this study.

If SEU cross sections are sensitive to ion velocity as well as to LET, tests using these beams will detect a difference in SEU cross section for two different ions with overlapping ranges of LET. That a velocity dependence could exist is due to the difference in the ion track density[6] of two ions with the same LET but different velocities. As an example, a 30 MeV/amu neon ion has about the same LET as a 450 MeV/amu iron ion. The secondary electrons in the neon track will, however, have lower energy than the iron's since the iron ion has a much higher velocity. (The details of the charge distributions around ion tracks can be calculated using Monte Carlo models based on measured secondary electron emission data.) The neon track will then initially be denser and have a longer lifetime as it undergoes ambipolar diffusion. Whether or not a given device will be sensitive to the differences in track structure can not yet be estimated due to a lack of detailed knowledge of charge transport in the track after the secondary electrons have reached thermal equilibrium with the silicon lattice. If significant deviation from the secant law exists, the impact on predicted error rates could be large since the integral LET spectrum in space, the "Heinrich curve",[7] is a strong function of LET. Small changes in measured critical LET with incidence angle or a species dependence can lead to erroneous estimated error rates.

Experimental Technique

The facility used for these tests was the Berkeley Bevalac. This facility has the capability to produce ion beams of heavy particles of relativistic energy. As seen in figure 1, high energy heavy ions can be used to cover a wide span of stopping powers (LET). The range of the ions is also quite long, permitting adjustment of the output LET with a variable thickness absorber (a water column). Further, the energy of the ions are similar to the energies of cosmic ray particles. This facility is used extensively to generate particles for cancer therapy. Consequently, precise techniques[8] have been developed for beam diagnostics, dosimetry, and control. We have applied these techniques to SEU studies. These techniques are summarized below.

The experimental apparatus is shown in figure 2. The incident ion beam is passed through lead scattering foils to increase the lateral size of the beam. Beam alignment and width are monitored using the two segmented, parallel-plate ion chambers. For 600 MeV/amu Fe, 6/64 inches of Pb foil produced a Gaussian beam at the sample with a full-width-at-half-maximum of 12 cm. Once the beam is aligned and widened a Bragg curve (figure 3) is measured by placing a third ion chamber downstream of the water column. The penetration depth to the Bragg peak determines the maximum beam energy reaching the target. Only penetration depths less than the Bragg peak are usable with this delivery and monitoring system, as will be explained below. The water column can slow a beam over a range of LET values from 1.7+/-0.1 to 15.0+/-0.7 MeV/(mg/cm^2) for incident 600 MeV/amu Fe. The range of LET values for incident 670 MeV/amu Ne is 0.6+/-0.003 to 2.0+/-0.2 MeV/(mg/cm^2). The LET of the beam striking the target is then adjusted by setting the water column thickness such that the beam exiting the water column could penetrate a distance into a water tank that corresponds to a desired ion energy and

LET. Corrections are made for lid thickness, air path, and specific stopping power of water verses silicon.

The width of the Bragg peak is dominated by range straggling and is proportional to initial energy. As the primaries begin to reach their end of range, over a depth proportional to the incident energy, the LET distribution grows quite wide, from stopping ions to those that have about 5% of the initial energy. For this reason the practical upper limit on LET is the LET at the peak of the Bragg curve. LET as a function of distance (equivalent water thickness) from the Bragg peak is shown in Figure 5. This indicates the accuracy with which the Bragg peak can be placed in the sensitive volume of a device. The water column can be set to an accuracy of +/- 0.005 cm. So the penetration distance to the Bragg peak should be selected to be greater than 0.005 cm for a maximum LET of 15 MeV/(mg/cm^2) for iron. Finally, near the Bragg peak, the LET is a distribution produced by range straggling, as described above, however no correction is made for the width of the distribution. Only the flatness of the asymptotic cross sections given here, and in an earlier paper,[5] is evidence of the validity of not correcting for the LET spectrum width.

The ion fluence is calibrated with the third ion chamber at the sample position with the water column set a minimum thickness. Dose delivered to the third ion chamber is measured for a given dose on ion chamber two. Fluence is then computed using the dose measured by ion chamber two.[8]

$$dose = 1.602 * fluence * LET * E-5,$$

where fluence is measured in ions per square centimeter, LET in MeV/(mg/cm^2) and dose in rads.

In traversing the water column, almost all of the energy lost by the primary ions is lost through Coulomb collisions with bound electrons in the water. However, the primary ion species flux is slowly attenuated by collisions with hydrogen and oxygen nuclei of the water. The collisions, when they occur, fragment primary ions, attenuating the primary species, building up a population of lower atomic-number ions. Beam transport codes[9] can accurately compute the depth-dose curve resulting from a beam that is being slowed and attenuated. (See the attached document UCRL-17392 Revised. This document predates the inclusion of the Silberberg and Tsao fragmentation cross sections, but includes all other effects.) Figure 4 is a comparison of a Bragg curve measured with ion chambers[8] (triangles), measured with a particle identifier telescope[10] (solid circles), and calculated curve[9] (solid line). The secondary ions are shown as measured by the solid-state detector, each line labeled with the atomic number of the secondary. At the Bragg peak the contribution to the dose from all secondaries is about 20% of the total. The LET of the secondaries is much lower than the primaries both because LET goes as the atomic number squared and because the secondaries lose energy more slowly than the primaries. Thus at the Bragg peak the secondaries have lower LET because they have lower atomic number and because, due to their lower stopping power, they have lost less velocity. The agreement between measurements and calculation is within 5%. The primary ion is seen to dominate the dose (thus LET) till the primaries reach their end of range. Attenuation of the primaries is corrected for in the dose calculation.[5] The attenuation length of Ne in water is 18 cm, and for Fe is 9 cm.

The test system consists of a DEC PDP11/73, running extensive test software based on Micropower Pascal. The system provides test pattern output to the test device.

automatic control of the Bevalac parameters including dose, beam current, and water column thickness, as well as calculations of the results in terms of cross section at each value of LET.

Upset measurements are performed with the third ion chamber removed and replaced by the device(s) under test (DUT). Beam alignment and size are continuously monitored by the two upstream ion chambers. Upsets per dose on ion chamber 2 are recorded. Fluence is computed based on dose to ion chamber 2 and the primary ion attenuation in the water column. LET is computed based on the measured Bragg peak depth, air path to the DUT and the DUT lid thickness. Any system dead time, such as device read/write time, is factored into the fluence calculation in real time.

The DUT's were irradiated at fixed beam incidence angles. For all but the parallel incidence, the LET is scanned at each angle. For parallel incidence, only maximum energy beams were used because the stopping power of the beam would change across the width a device at low energy.

The irradiation of the RCA ALU was conducted with a modified iron ion beam. The beam energy spectrum was spread from maximum incident energy to stopping. The spectrum was produced by passing the ion beam through a brass plate machined to have an area distribution of thicknesses that was proportional to the relative population of ions with energies corresponding to the incident range minus the thickness of the plate. A Bragg curve of the resulting beam is shown in figure 6 with the calculated galactic cosmic ray iron depth-dose distribution shown for comparison. The curves are in good agreement. Differences are due to ignoring scattering in designing the range modification plate. The average LET of the beam at zero water column depth is about 2 MeV/(mg/cm2). The energy

distribution is approximately sinusoidal with the relative flux being zero at zero and maximum energy and is maximum at about 300 MeV/amu.

Results

Three bipolar RAM's were studied, the 93L422, the 27S03, and the 27LS00. Two of the 93L422 parts were delidded. Due to a high mortality rate in the delidding process, the remaining parts remained lidded. Figure 7 is a plot of the SEU cross section for four 93L422's. Each symbol is the average of two devices, either lidded or delidded, under three irradiation conditions. Error bars (counting statistics only) are the size of the symbols except at the lowest cross sections where only tens of events were measured. (Note that at the lowest LET's the LET is best defined since these points are at the thinnest water column thicknesses and thus have the lowest secondary particle contamination.) This data is in agreement with the previously published data for this device.[11] As noted earlier the measured asymptotic cross section is flat above LET of 3 MeV/(mg/cm^2) implying that the contribution from the increasing population of lower atomic-number secondary ions is dominated by the contribution from the surviving primaries. (At greater depths. the LET becomes ill defined with some primary particles having slowed past the peak of the LET curve and some yet to slow to the peak LET. The spectrum of LET past the Bragg peak then ranges from about half the maximum to the maximum single particle LET.)

The results for each of three 27LS00's, shown in figure 8. The LET thresholds display both a pronounced species dependence and a noticeable incidence angle dependence. The data for each device is shown separately. Each data point represents more than 100 events per device except at the lowest cross sections where tens of events were recorded. The resulting plots show groupings by species and by incidence angle, within error limits. The curious dip in the iron data at an LET

of four is as yet unexplained. No anomalies in dosimetry were found nor did SPICE modeling of the memory cell reveal any anomalous transient behavior in the region between LET values of 3 to 5.

As noted in the discussion of figure 4, for water column depths less than the Bragg peak, the total dose, composition, and beam-averaged LET are known to better than 5%. The beam in figure 4 is the worst case of those used in this study. There the beam undergoes the most fragmentation (only 15% of the incident primaries survive to the end of range) and the incident energy is the highest used (670 MeV/amu) giving the greatest range straggling. If there was a systematic error in LET, then when the hypothetical correction is applied to the 93L422, that device would show a species dependence. In the case of the 27LS00, the range of the Fe at threshold is over a centimeter. The LET at that point in the Bragg curve is known to within a percent. The LET of the Ne beam cannot be greater than 2 MeV/(mg/cm^2) due to range straggling restricting how close to the Bragg peak LET is defined. Or, in other words, the population of ions with LET greater than 2 MeV/(mg/cm^2) are spread out over a range in water column thicknesses such that there are very few stopping ions with LET greater than 2 at any one water column setting. Thus the SEU threshold measured using Ne must be less than 2 MeV/(mg/cm^2) and using Fe is at about 3 MeV/(mg/cm^2). We conclude that a significant species dependence exists for the 27LS00.

The results for the AM27S03 are shown in figure 9. The device is similar to the AM27LS00 but lacks the Schottky clamp. The LET threshold is higher than for the 27LS00 but has the same asymptotic cross section. The effect of the Schottky clamp on the 27LS00 device is seen to reduce the critical charge, all other variables held constant, as expected. An additional test was run on the CMOS equivalent of the

27S03, the Cyprus 189. The data is plotted in figure 10. This newer device is shown to have a smailer asymptotic cross section per bit, but a threshold about half that of the 27S03. In the galactic cosmic ray environment, the lower threshold would increase the number of ions the device would be susceptible to by a factor of ten. But, since the measured cross section is down by two orders of magnitude, the total SEU rate from GCR's would be a factor of ten less for the CMOS than for the bipolar device.

Permanent damage was not detected in any of the parts. Power supply current was monitored throughout the tests and seen to not vary. This is in agreement with the fact that the total dose to the parts was on the order of 100 rad.

Multiple-bit upset by single ions was reported earlier.[5] In that study it was found that the multibit half angle in the 27LS00 is +/- 15 degrees from parallel incidence. In this report we mapped the logical address verses physical location for the 93L422 and the 27LS00 using a finely focused laser.[12] The memory maps for the 93L422 and the 27LS00 are appended to the COTR's report. Note that the 93L422 device 4 has all apparent double-bit errors due to a stuck address line. The data for device 4 was corrected for this fault. Figures 11 and 12 are memory maps of the 93L422 with upset bits shown as "+" for zero-to-one transitions and "-" for one-to-zero. The first case is for the ion beam incident along the long axis of the device. The result is a single row of upset bits. On the average, there were 5.6 errors per single ion striking the active areas. The second case is for a beam incident along the short axis of the device. The result is a double row of errors with an average of 11 errors per event. This result shows that multiple errors from a single strike may occur in a cosmic ray environment.

The 93L422 bit cross section at parallel incidence is 6.5 x 10-5 cm^2 for incidence along the short axis of the memory cell and 1.8 x 10-5 cm^2 along the long axis. When the short-axis data is corrected for correlated bit hits (i.e., divided by 2), the sensitive depth per bit is 60 microns for parallel incidence. This is a surprisingly large depth. It implies that charge from the track may drift for long distances before being collected. This is in agreement with the normal incidence data for the 93L422 where in, for example, run #1 there are 14 single bit-errors, 5 double-bit errors, and 9 triple-bit errors. If error addresses were uncorrelated, then there would be only (8 in 1024) double-bit errors per single bit error, and triple-bit errors would be very rare. The large number of double- and triple-bit errors imply that the errors are correlated, supposedly by a finite track width that can overlap two or more bits. The off transistors are separated by distances on the order of 50 to 100 microns and are 30 x 50 microns. Thus the large sensitive depth for parallel incidence and the high rate of multibit errors at normal incidence are consistent and imply track widths on the order of 50 microns.

The 27LS00 exhibits fewer than 3 double-bit errors per 100 single-bit errors for normal incidence beams. The total memory area is 2.1×10^{-2} cm^2 verses an asymptotic SEU cross section of 1.5×10^{-2} cm^2 so the relative density of bits is similar to the 93L422. The doping profiles for the 27LS00 are not known to us, but may explain the different behavior of the 27LS00 to the 93L422.

Parallel incidence beams on the 27LS00 produced multiple errors per ion, but at lower linear density than with the 93L422. Frequent, large gaps in the rows of errors are common, as shown in figure 12 . This is consistent with the normal incidence beams where neighboring bits do not suffer simultaneous upset frequently with respect to the 93L422 case. The physical mechanism that provides a barrier against multibit upset,

as opposed to that seen in the 93L422, is not known. The results for the RCA ALU test are given in a separate paper.[13]

Discussion

The multibit phenomenology described in this report are in qualitative agreement with recently published flight data by Blake and Mandel[2] and disclosed by Smith.[3] Multibit upset occurs in RAM at about 10% of the single-bit upset rate and strings of upset bits are observed occasionally. These multibit upset represent a survivability threat to military and commercial space systems. The new generation communication satellites such as TDRS and INTELSAT 6 are and will, for their full series of the present design, continue to be susceptible to lifetime shortening due to multibit upset contributing to erroneous station-keeping motor firing. New design requirements need to be specified for future spacecraft that will reduce the impact of multibit SEU.

The possible occurrence of a species dependence in the 27LS00 was first reported in 1984.[5] Only a single device was measured at that time. This report is based on three devices with the same date codes. The cross section data are nearly identical for the three devices. The basis of a species dependence could be differences in recombination along the two tracks or the difference in ion track structures. Track structure is a description of the radial ionization profile. The core of an ion track is very densely ionized, approaching full ionization of nearest neighbor target atoms along the ion track. Recombination should be greatest at the highest ionization densities. Since the two ions have about the same ionization densities at the core of the track, recombination, if it exists at all, should be the same for both ion tracks. To first approximation, the radial energy density (ionization) distribution falls off as the inverse-square of the radius.[14] Variations from the

inverse-square are due to the kinematics of the ion-bound electron pair. Two ions can have the same stopping power (or unrestricted LET) and produce different tracks. Take, for example, the case where the beams emerging from the water column have been slowed to energies such that both have LET's of about two (i.e., where there is a large separation between Ne and Fe SEU cross sections for the 27LSOO). The energies are 30 MeV/amu for Ne and 450 MeV/amu for Fe. The track of the Ne ion consists of relatively low energy ionized electrons ejected nearly isotropically from the struck atom. The ionized electrons from the Fe collisions are much higher energy (i.e., as high as 4 MeV). The high energy electrons leave the local volume in the forward direction carrying some fraction of the energy lost by the Fe ion away from a site the size of a typical junction (20x20x10 microns). These high energy electrons are relatively infrequent but are clearly visible in photographic emulsions as "spurs" sticking out from the dense core. (See the photographs in an early SEU paper.[15]) The tracks are seen to be qualitatively different.

Figure 13 is a plot of the radial energy densities of equal-LET Ne and Fe. The plots are from a Monte Carlo calculation based on measured secondary electron cross sections.[6] Over much of the range in radius the Ne energy density is slightly higher than the Fe density. At about a micron the Ne density distributions falls off rapidly while the Fe distribution extends to past ten microns. The integral over these curves give the stopping power of the ions. (In practice, all dosimeters have a finite volume and some radiation escapes detection. In that case a restricted LET is defined that is the integral from zero to some finite energy that is known to be captured.) For this case of LET equal to about 1.7 MeV/(mg/cm^2), a log (relative energy density) of -2 is equal to 10^{16} electron-hole pairs per cubic centimeter. The log-log plot is difficult to read, but the difference in energy density between the Fe an Ne tracks is about a factor of 1.4 at this density. Since the Debye screening

length is large compared to the radius, the core of the track is well shielded from the applied fields. Thus, most of the electron-hole pairs that participate in the SEU current pulse are in the sheath at densities just above the dopant densities and are at the densities where the greatest differences in ionization density are between the Ne and Fe tracks. The source of the differences in energy density is shown in figure 14. The ratio of Ne to Fe ion secondary electron cross sections is plotted verses secondary electron energy (the cross sections are differentiated with respect to electron energy). At low energies the ratio of the cross sections is nearly unity. From 100 eV to 100 keV the Ne secondaries are more frequent. At higher energies there are only Fe secondary electrons (i.e., the Fe ion track secondary electrons have a harder spectrum). So, over radii from near zero to the median range of 100 keV electrons, the Ne ion track has higher ionization densities.

The effect of different ionization densities at levels near the dopant densities seen in the two devices tested may appear as a difference in the space-charge limited current drawn from the two tracks. The iron track would have a smaller radius at the background dopant density. Thus a smaller current could be supported by the Fe track. The SEU pulse profile should be measureably different for equal-LET Fe and Ne ions since the effects on a struck node differ. Further work should be undertaken to measure the pulse profile in 27LSOO and the 93L422 to confirm or deny the above argument.

Conclusions

Multibit SEU has been measured in two devices. The normal and parallel incidence response in the two devices are qualitatively different. Both are susceptible to MSEU, but the 93L422 is sensitive to strikes 50 to 100 microns away from the sensitive junctions yielding upset cross sections large compared to the known sensitive

junctions, while the 27LS00 sensitive area and MSEU cross sections are equal. A self-consistent and accurate test of SEU thresholds and cross sections measured at fixed incidence angles has been made on two bipolar devices. On the 93L422 the thresholds and cross sections were found to scale as the secant of the incidence angle as current models assume. On the 27LS00 the thresholds and cross sections were found to be dependent on ion species and to not scale as the secant of the incidence angle. A plausibility argument based on a Monte Carlo model of the ion tracks describes how a species dependence could exist. Other factors such as device characteristics have yet to be developed and applied to the model. Variations from the secant of the incidence angle could be due to depletion region geometries varying from that of a parallelepiped or from an angle dependent funnel effect. A larger data base will need to be developed to answer these questions.

Recommendations

Advances in test techniques at the Bevatron have significantly reduced the costs of testing parts there. Multiple parts and part types can be tested simultaneously over a broad LET range at one angle in less than ten minutes. Advantage should be taken of these techniques to broaden the part type data base on MSEU and species and angle dependence of SEU. Test structures should be exposed in order to determine the charge collection efficiencies and time profile of SEU from fast, heavy ions.

New theoretical models should be developed to explain the new MSEU phenomena. Effects of delayed charge collection due to ion track self-shielding need to be addressed.

Acknowledgments

The authors wish to thank the staff of the Lawrence Berkeley Laboratory Bevalac for their friendly, enthusiastic support in carrying out this study. Thanks are also given to DNA/NRL for funding this program.

References

1. D. Vinson, Proc. Spacecraft Anomalies Conf., Colorado Springs, Co., October 30-31, 1984, V. G. Patterson and J. S. Schleher editors, pp. 94-109.

2. J. B. Blake and R. Mandel, IEEE Trans. Nucl. Sci. NS-33, 1616 (1986).

3. E. C. Smith, private communication.

4. R. Peters, INTELSAT, private communication.

5. T. L. Criswell, P. R. Measel, and K. C. Wahlin, IEEE Trans. Nucl. Sci. NS-31, 1559 (1984).

6. W. E. Wilson and T. L. Criswell, Adv. Space Res., 6, 75 (1986).

7. W. Heinrich, Radiation Effects, 34, 143 (1977).

8. J. T. Lyman, Radiation Dosimetry, vol. III, Ed. Frank Attix and Eugene Tochlin, Academic Press, New York, 1969.

9. G. Litton, J. T. Lyman, and C. Tobias, University of California Radiation Laboratory Report, UCRL-17392, Rev. (1968).

10. J. Llacer, Med. Phys. 11, 266 (1984).

11. D. K. Nichols, W. E. Price, W. A. Kolasinski, R. Koga, J. C. Pickel, J. T. Blandford, Jr., and A. E. Waskiewicz, IEEE Trans. Nucl. Sci. NS-32, 4189 (1985).

12. A. K. Richter and I. Arimura, IEEE Trans. Nucl. Sci. NS-34, 1234 (1987).

13. G. J. Brucker, P. Measel, D. Oberg, J. Wert, and T. Criswell, IEEE Trans. Nucl. Sci. NS-34, 1792 (1987).

14. R. Katz,S. C. Sharma, and M. Homayoonfar, Radiation Dosimetry, Supplement 1, Ed. Frank Attix and Eugene Tochlin, Academic Press, New York, 1969.

15. W. A. Kolasinski, J. R. Blake, J. K. Anthony, W. E. Price and E. C. Smith, IEEE Trans. Nucl. Sci. NS-26, 5087 (1979).

Figure Captions

Figure 1. The stopping power of heavy ions is double valued verses energy. A broad span in stopping power can be covered by a single relativistic ion species. The incident cosmic ray spectrum for Fe is shown verses energy.

Figure 2. The Bevalac test configuration consists of Pb foils to widen the beam, ion chambers to monitor beam alignment, size and dose, variable-thickness water column to slow the incident beam and a device support and test system.

Figure 3. The Bragg curve is used to calibrate the maximum incident energy and maximum attainable LET.

Figure 4. The composition and beam-averaged LET can be measured with solid-state detectors or computed by transport codes to high accuracy. The results can be compared to a Bragg curve measured at the time of the experiment to calibrate the LET of the primary ions striking to within 5%.

Figure 5. The results of the transport code modeling is a curve of LET verses distance from the Bragg peak. There is a separate curve for each ion and initial ion energy.

Figure 6. The measured depth-dose curve produced with a "energy filter" is in good agreement with that calculated with a transport code.

Figure 7. The SEU response function for the 93L422 is seen to scale as the secant of incidence angle and exhibits no species dependence.

Figure 8. The SEU response function for the 27LS00 exhibits a pronounced species dependence of the threshold and does not scale as the secant.

Figure 9. The SEU response of the AMD 27S03 exhibits the expected higher threshold due to the lack of a Schottky clamp.

Figure 10. The CMOS equivalent of the 27S03 has a lower SEU threshold but has a much lower asymptotic cross section.

Figure 11. An ion incident from the left has left a row of upset bits along its track. The "+" means a zero-to-one transition and the "-" a one-to-zero.

Figure 12. An ion incident parallel to the plane of the device and from the top leaves a double row of upset bits, implying that the device layout has overlapping cells in this direction.

Figure 13. The radial energy distributions around 30 MeV/amu Ne and 450 MeV/amu Fe. Both ions have LET of about 1.7 MeV/(mg/cm^2)). The iron track is below the neon out to a micron. Beyond a micron the higher energy secondary electrons produced by the iron ions predominate.

Figure. 14. The ratio of singly differential cross sections for secondary electron production by neon verses iron is plotted against secondary electron energy. It is seen that over the range in energies that correspond to where the neon track is denser than the iron track that the electron production by neon is 1.3 times that by iron.

Iron Spectrum

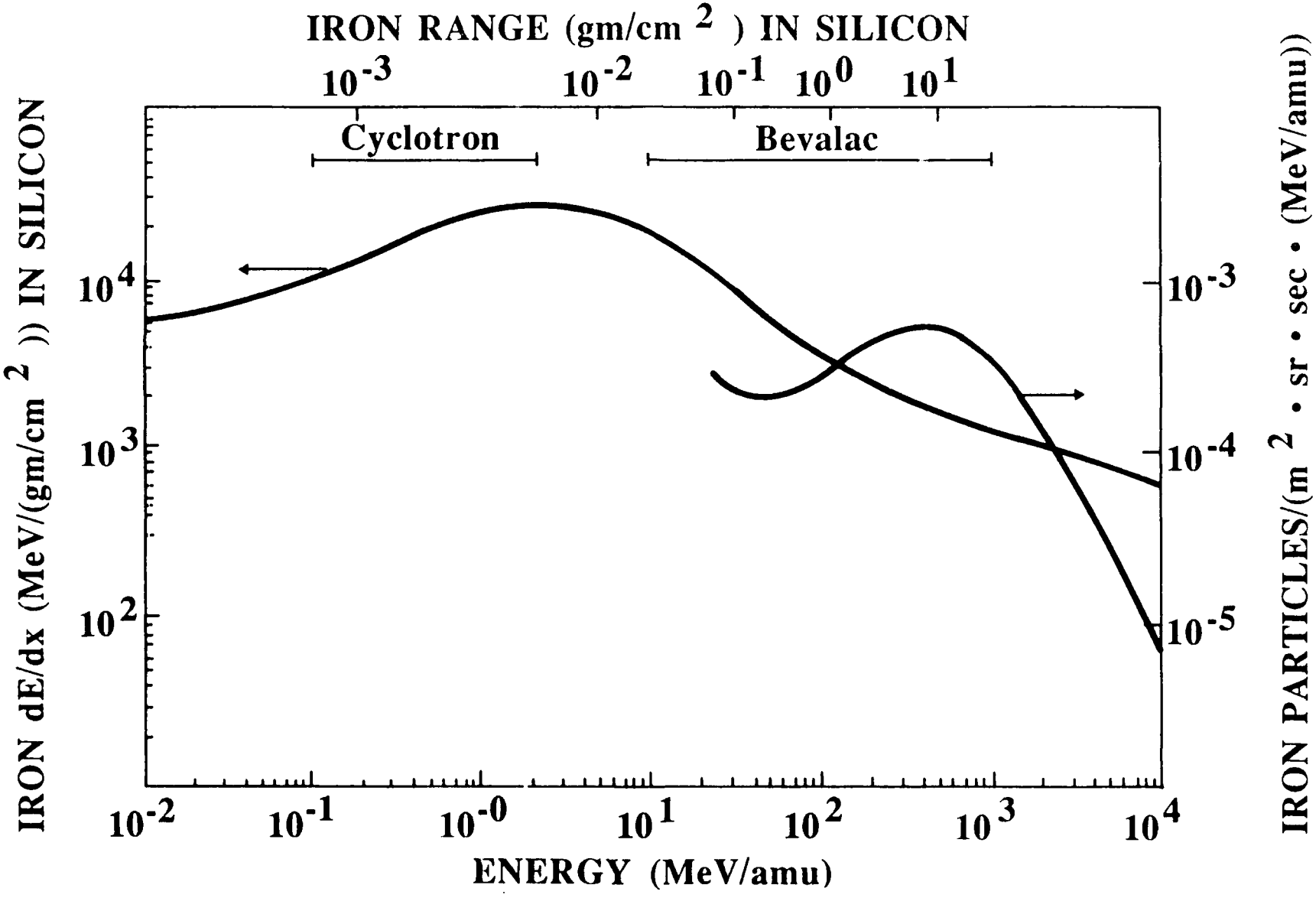

Figure 1

Bevalac Test Configuration

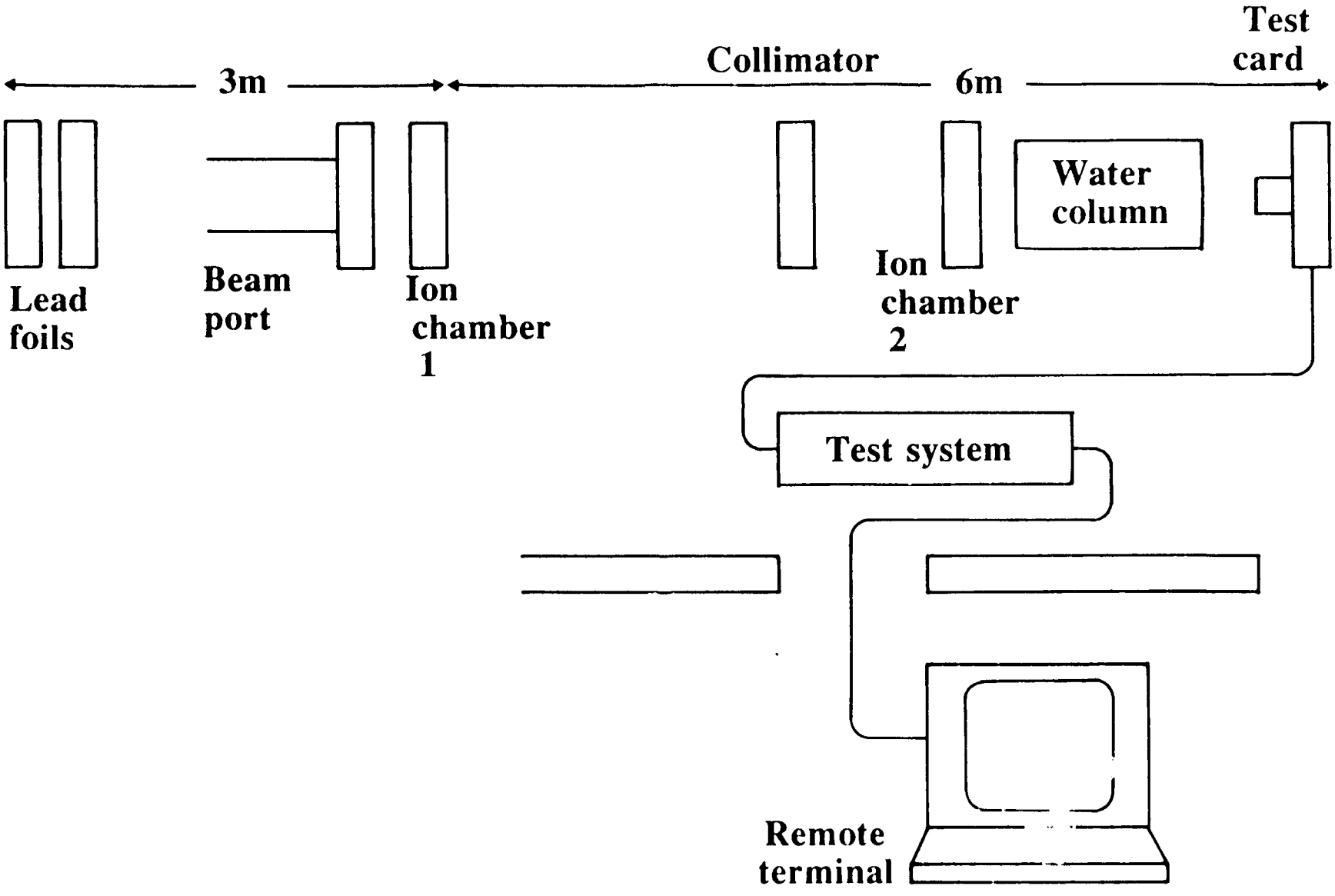

Figure 2

Bragg Curve for 600 MeV/amu Iron

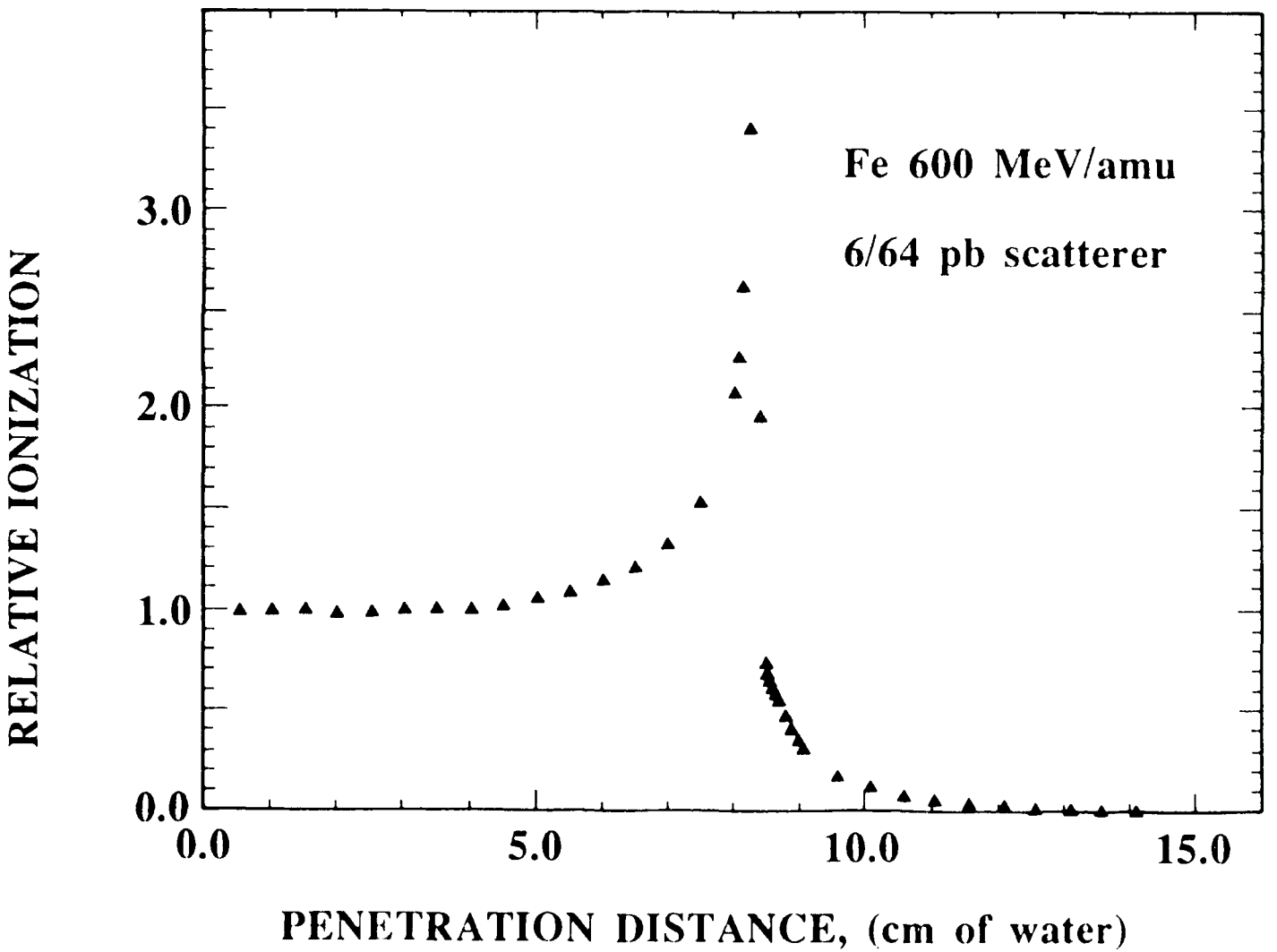

Figure 3

Bragg Curve

Ne 670 MeV/amu 8/64" Pb

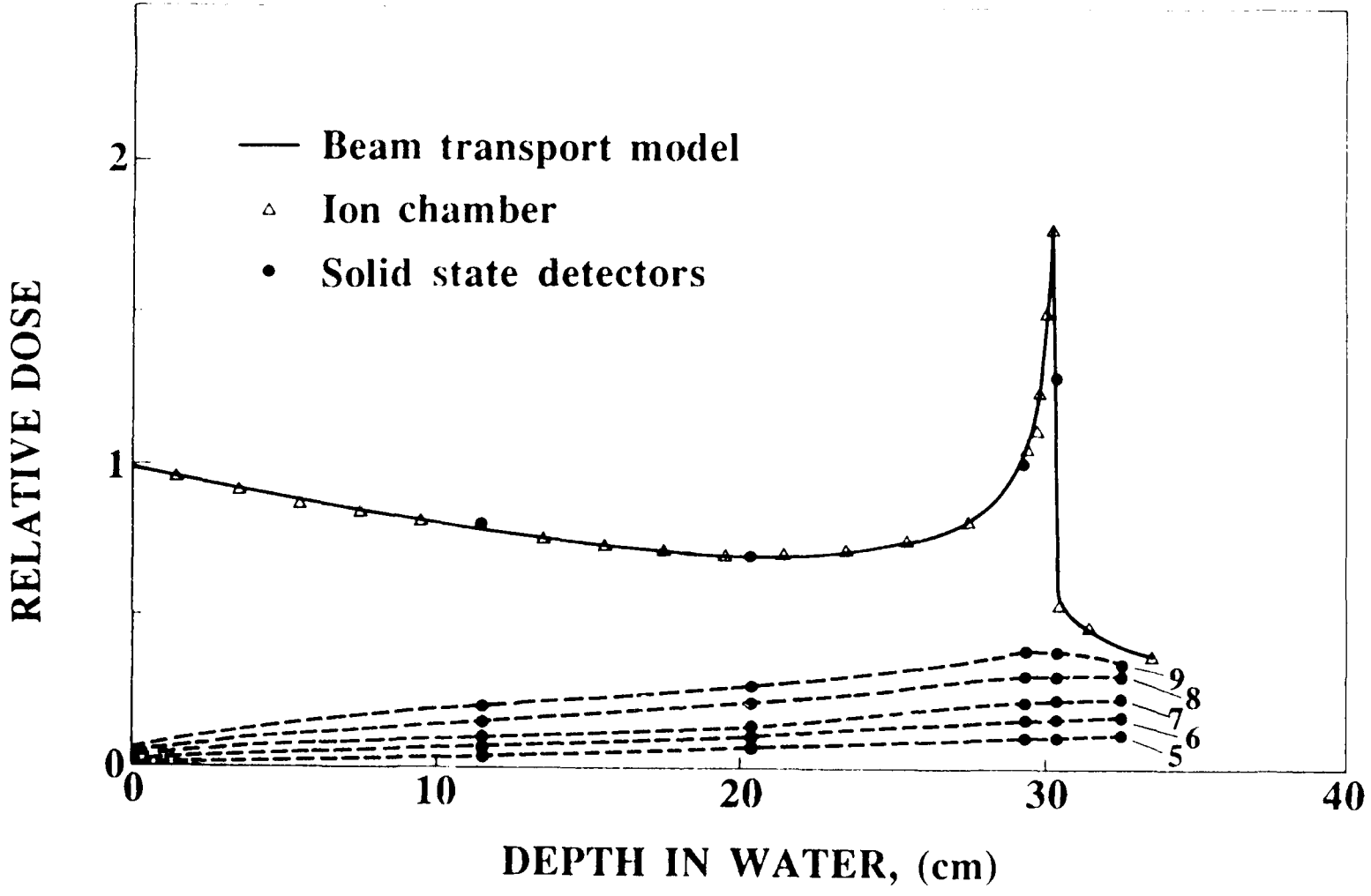

Figure 4

LET Functions

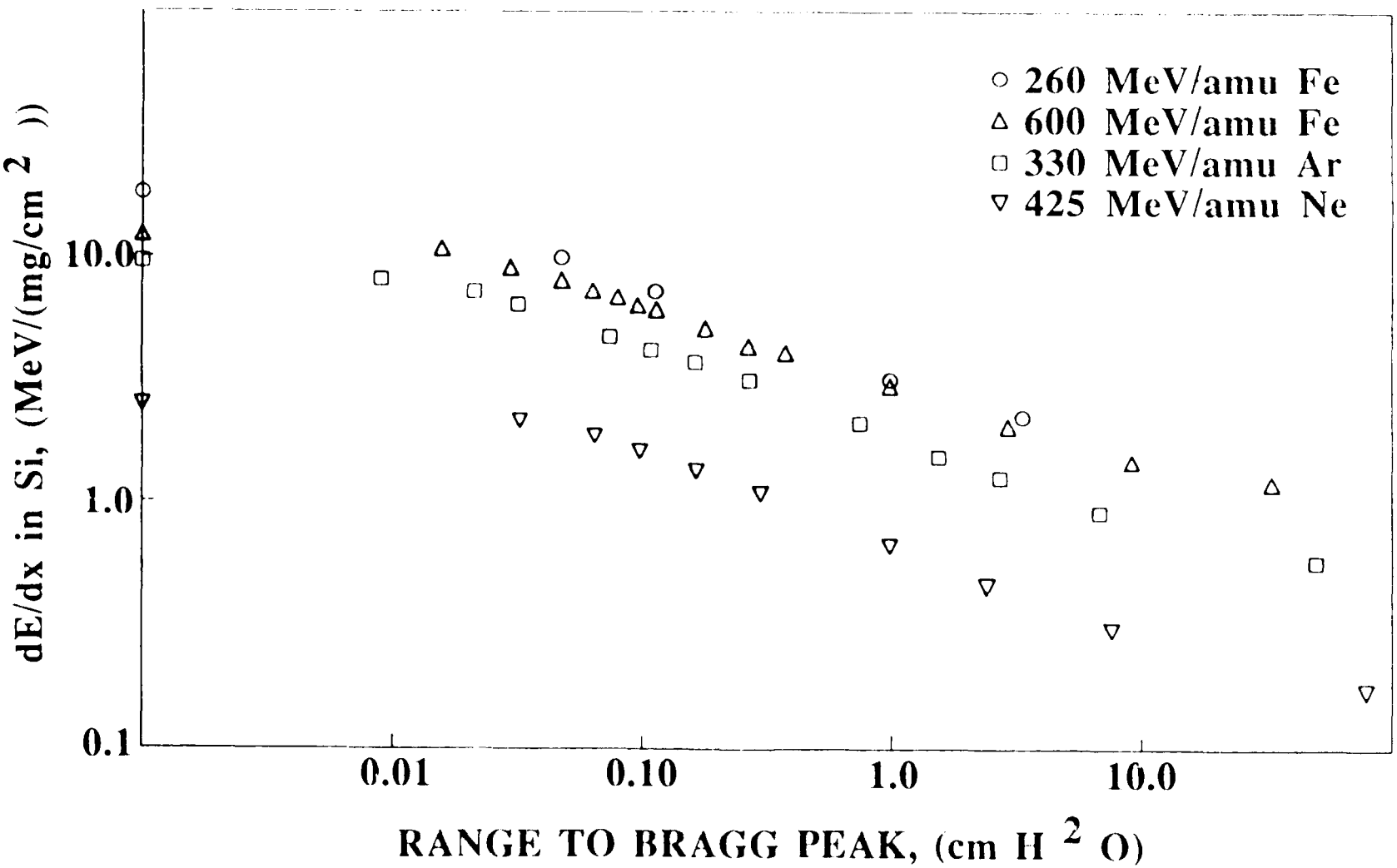

Figure 5

Galactic Cosmic Ray Spectrum

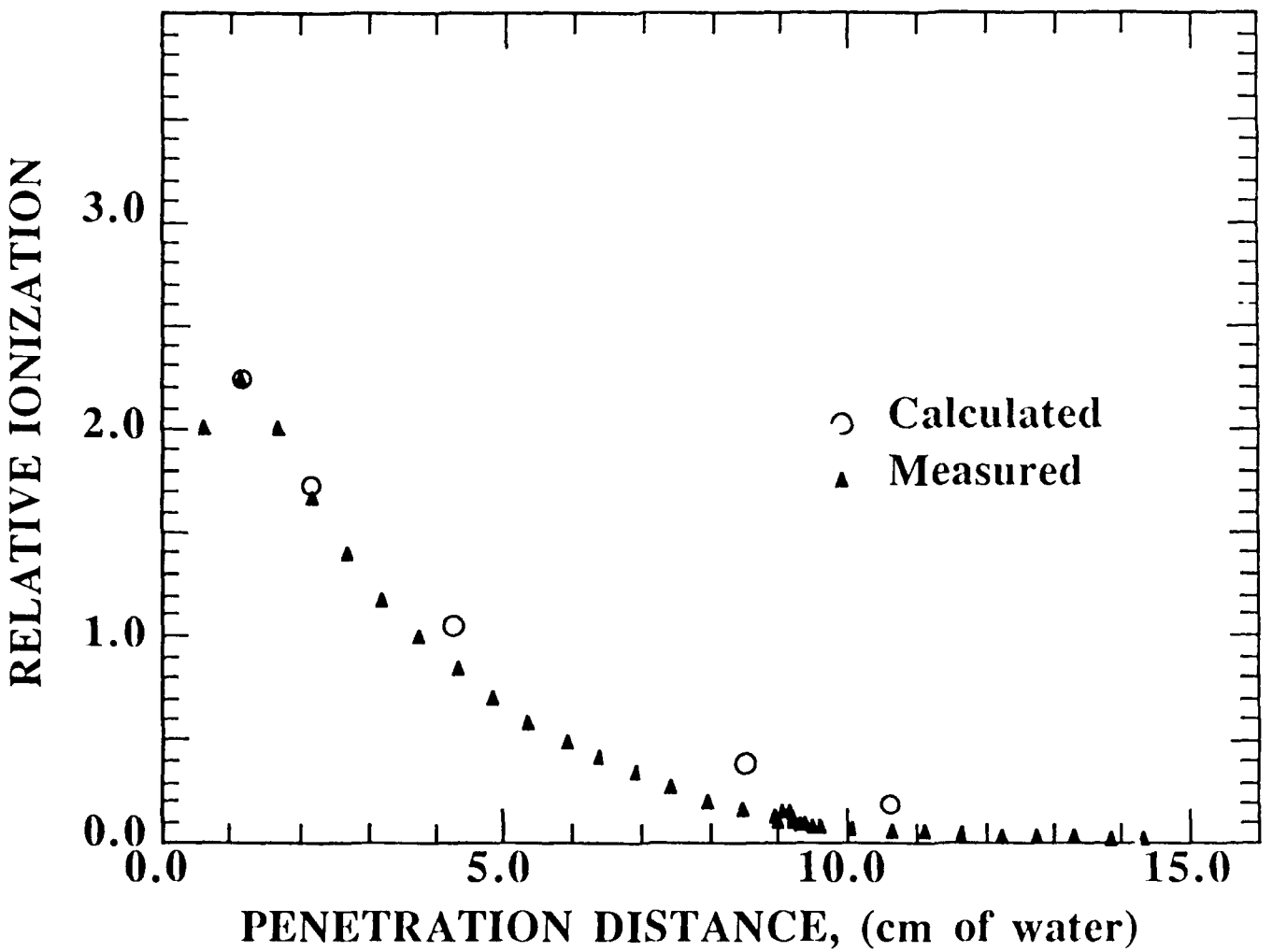

Figure 6.

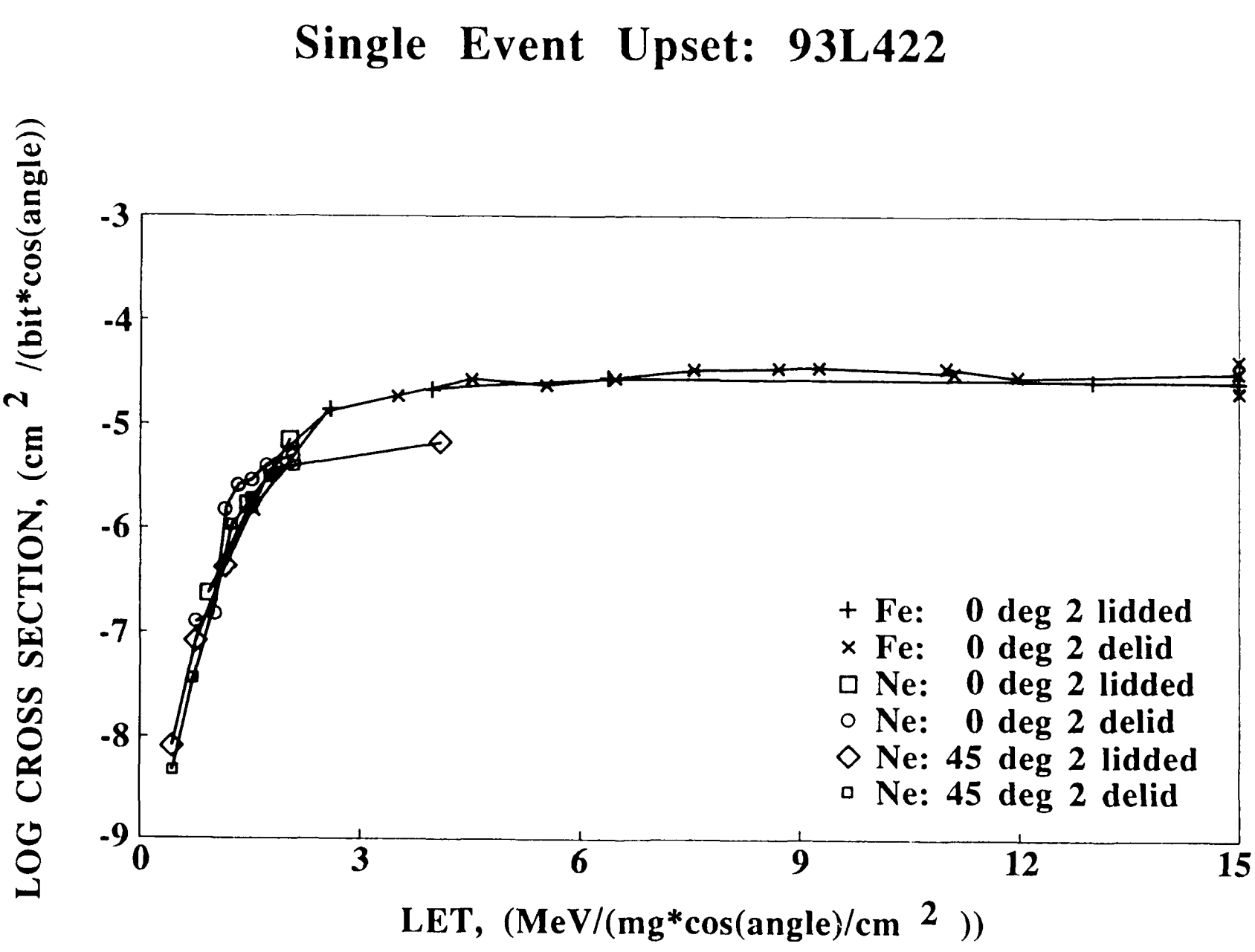
Single Event Upset: 93L422
LOG CROSS SECTION, (cm 2 /(bit*cos(angle))
-3
-4
-5
-6
-7
-8
-9
0
3
6
9
12
15
LET, (MeV/(mg*cos(angle)/cm 2))
+ Fe: 0 deg 2 lidded
× Fe: 0 deg 2 delid
□ Ne: 0 deg 2 lidded
○ Ne: 0 deg 2 delid
◇ Ne: 45 deg 2 lidded
▫ Ne: 45 deg 2 delid

Figure 7.

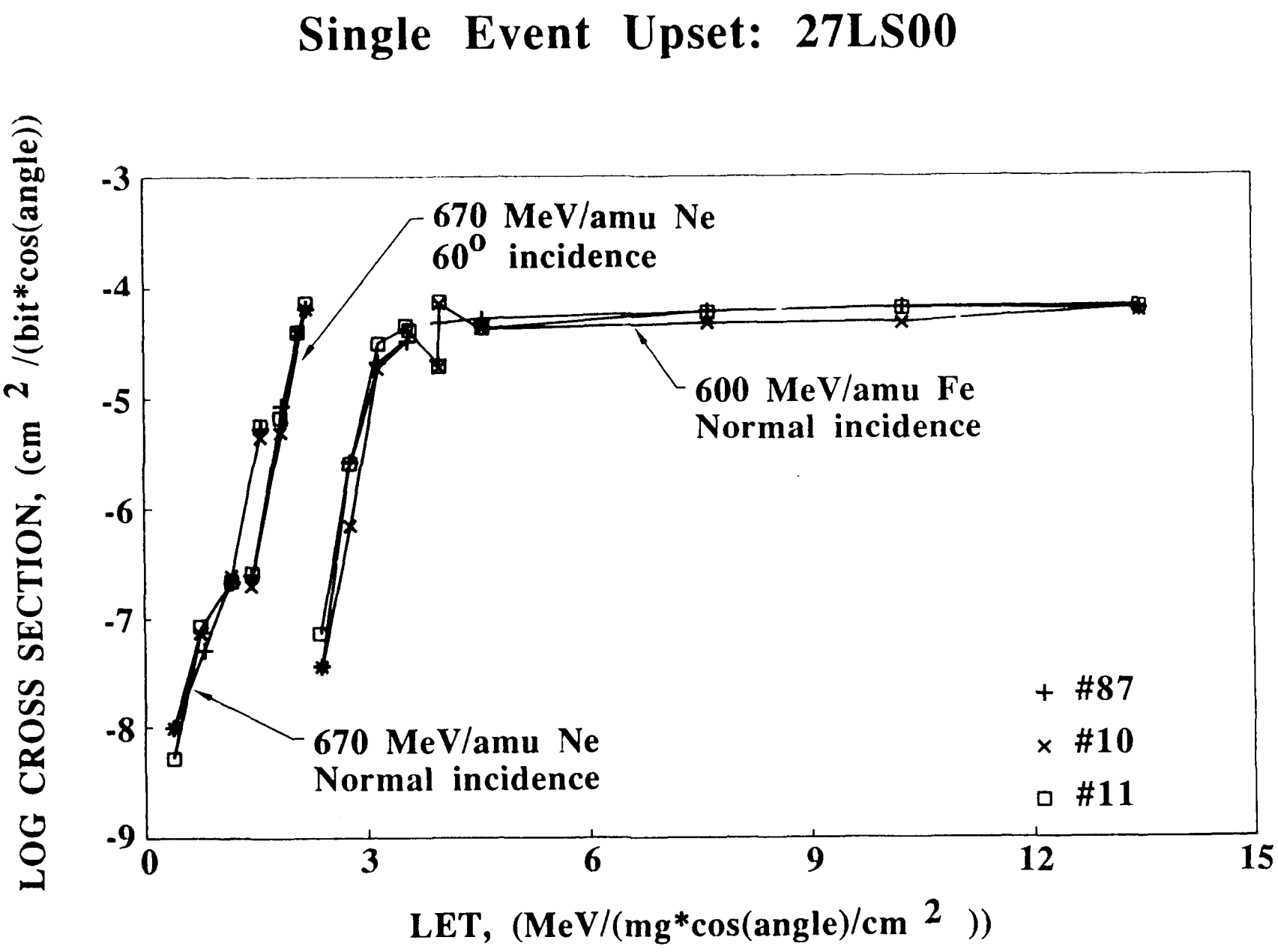
Single Event Upset: 27LS00
LOG CROSS SECTION, (cm 2 /(bit*cos(angle))
-3
-4
-5
-6
-7
-8
-9
0
3
6
9
12
15
LET, (MeV/(mg*cos(angle)/cm 2))
670 MeV/amu Ne
60o incidence
600 MeV/amu Fe
Normal incidence
670 MeV/amu Ne
Normal incidence
+ #87
× #10
□ #11

Figure 8.

Single Event Upset: AM27S03

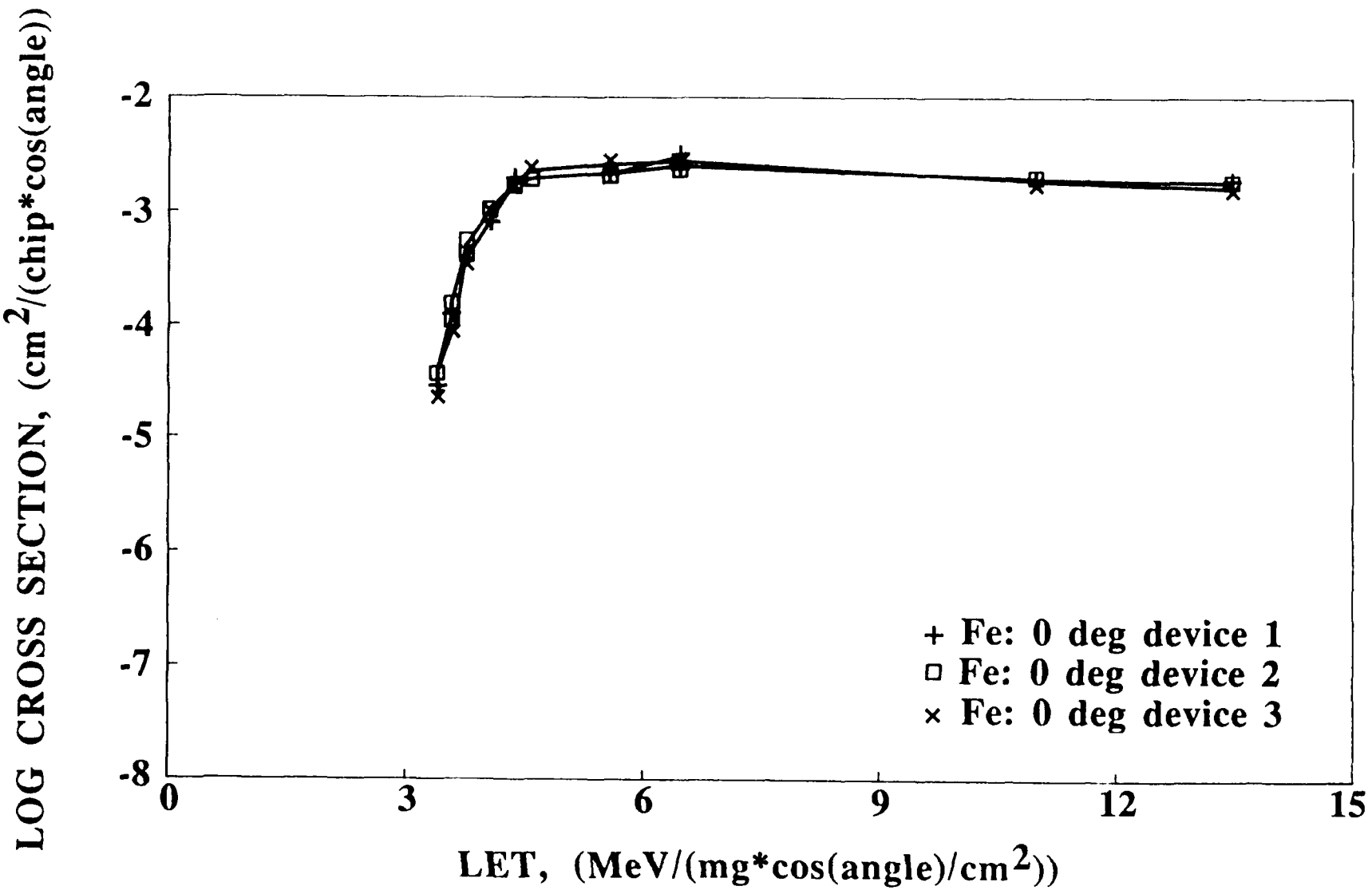

Figure 9.

Single Event Upset: Cyprus 189

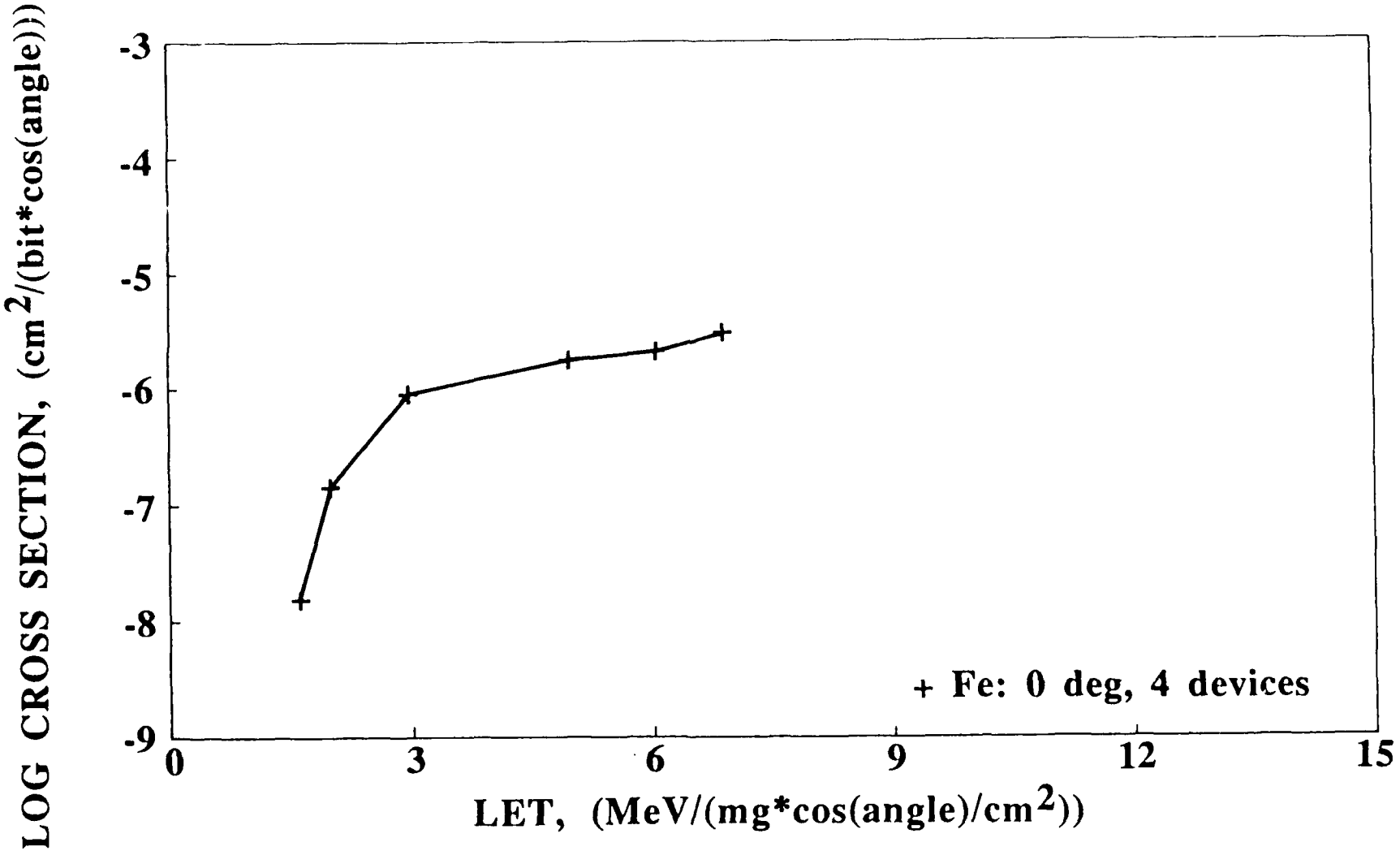

Figure 10.

Memory Map of 93L422

	Bit #1	Bit #2	Bit #3	Bit #4
	0123456789ABCDEF	0123456789ABCDEF	0123456789ABCDEF	0123456789ABCDEF
0				
1				
2				
3				
4				
5				
6				
7	++--++--++--	+ -	+	- +
8				
9				
A				
B				
C				
D				
E				
F				

600 MeV/amu Fe

Incident Edge-On, Let = 2.4 MeV/(mg/cm ^{2})

Figure 11.

Memory Map of 93L422

	Bit #1	Bit #2	Bit #3	Bit #4
	0123456789ABCDEF	0123456789ABCDEF	0123456789ABCDEF	0123456789ABCDEF
0			++	
1			++	
2			++	
3			++	
4			++	
5			++	
6			++	
7			++	
8			++	
9			++	
A			++	
B			+	
C				
D				
E				
F				

600 MeV/amu Fe

Incident Edge-On, Let = 2.4 MeV/(mg/cm ^{2})

Figure 12.

Radial Energy Deposition Distributions

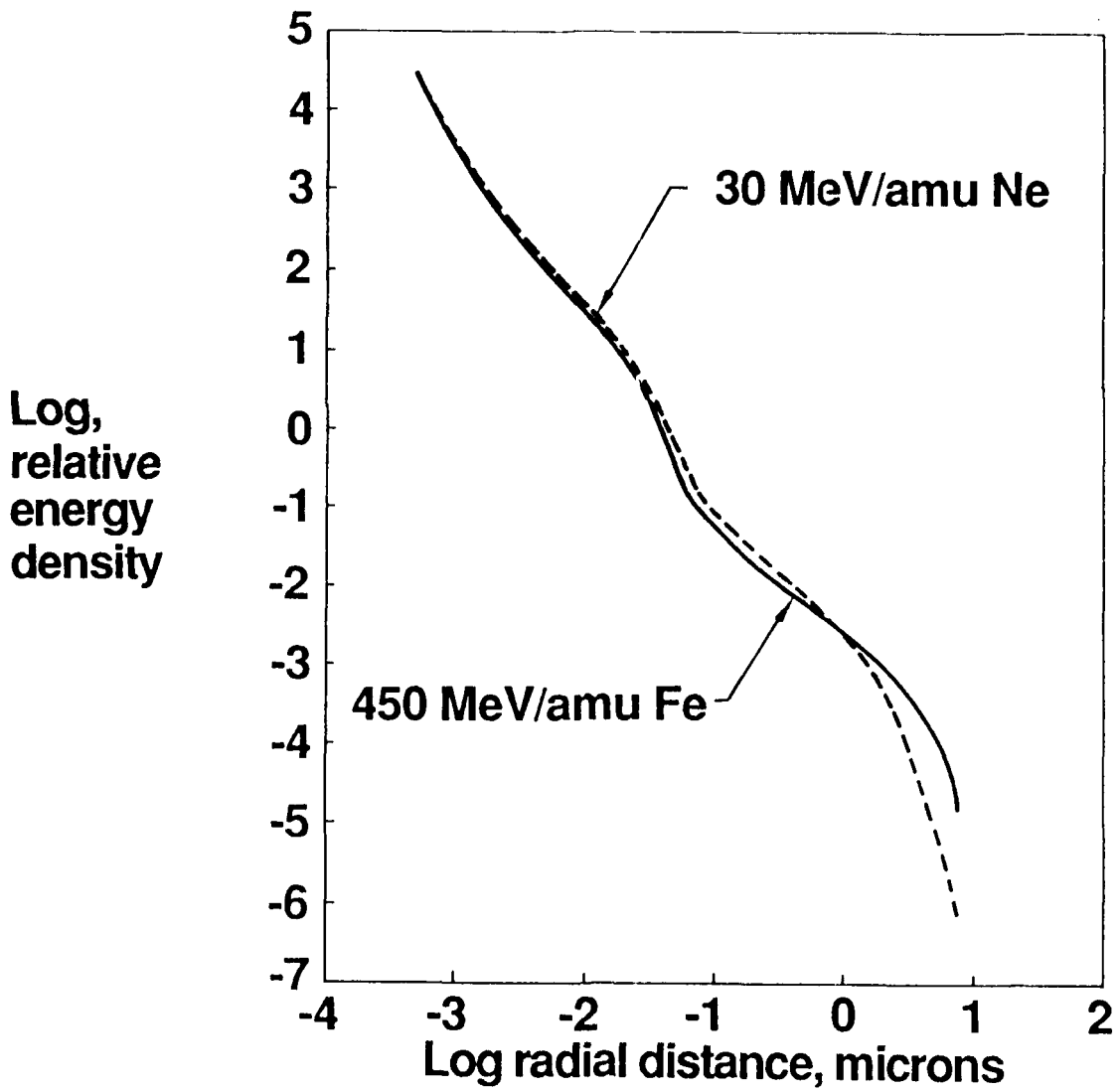

Figure 13.

Ratio of SDCS's neon/iron

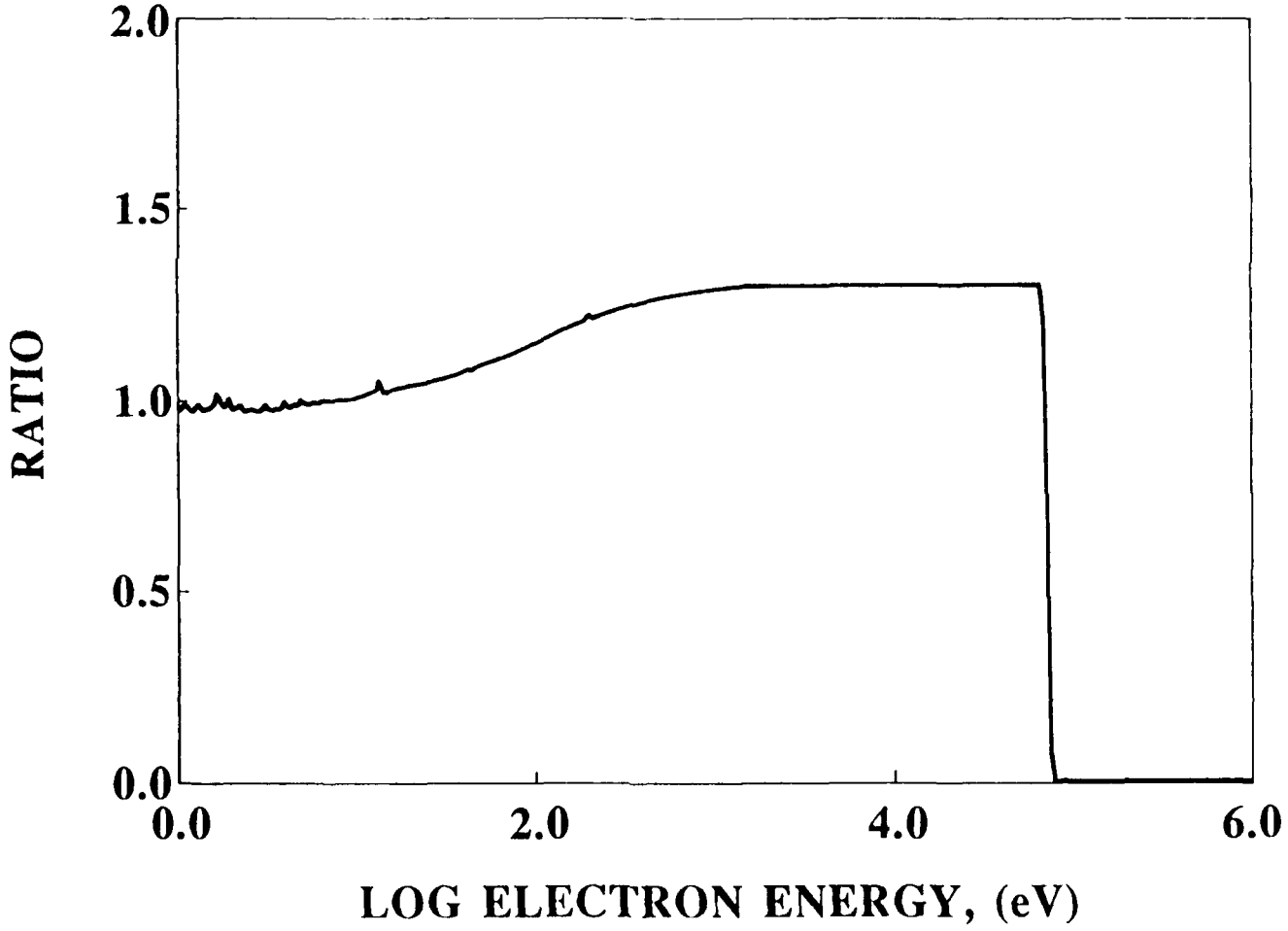

Figure 14.